Ultrahigh-Q Guided Mode Resonances in An All-dielectric Metasurface

Lujun Huang
UNSW Canberra
Rong Jin
Shanghai Institute of Technical Physics, Chinese Academy of Sciences
Chaobiao Zhou
Guizhou Minzu University
Guanhai Li
Shanghai Institute of Technical Physics, Chinese Academy of Sciences https://orcid.org/0000-0002-2745-055X
Lei Xu
University of New South Wales https://orcid.org/0000-0001-9071-4311
Adam Overvig
City University of New York
Fu Deng
South China Normal University
Xiaoshuang Chen
Shanghai Institute of Technical Physics, Chinese Academy of Sciences
Wei Lu
Shanghai Institute of Technical Physics
Andrea Alu
CUNY Advanced Science Research Center https://orcid.org/0000-0002-4297-5274
Andrey Miroshnichenko (andrey.miroshnichenko@unsw.edu.au)
UNSW Canberra https://orcid.org/0000-0001-9607-6621

Article

Keywords:

Posted Date: June 30th, 2022

DOI: https://doi.org/10.21203/rs.3.rs-1755479/v1

Version of Record: A version of this preprint was published at Nature Communications on June 10th, 2023. See the published version at https://doi.org/10.1038/s41467-023-39227-5.

Abstract

High quality (Q) factor optical resonators are indispensable for many photonic devices. While very large Q-factors can be obtained theoretically in guided mode settings, free-space implementations suffer from various limitations on the narrowest possible linewidth in real experiments. In these devices, the largest Q-factors are hindered by radiation loss induced by fabrication disorder. Complex photonic designs have been explored to enhance this response through either delicate engineering the topological features or carefully breaking symmetries. Here, we put forward a simple strategy to enable ultrahigh-Q guided-mode resonances in all-dielectric metasurfaces without breaking symmetry or carefully engineering topological quantities. We introduce a patterned perturbation layer on top of a multilayer waveguide system, aimed at exciting tailored guided-mode resonances from free space. We demonstrate that the associated Q-factors are inversely proportional to the perturbation squared, suggesting a simple way of achieving extremely high-Q resonances as the perturbation is reduced. The resonant wavelength can be conveniently tuned through material or structural parameters, such as the thickness and refractive index or the metasurface period, within a robust design strategy amenable for implementation in various platforms. We experimentally demonstrate such high-Q resonances at telecom wavelengths by fabricating a low-index photoresist layer photonic crystal slab on top of a 220nm top layer SOI substrate. The measurements show Q-factors up to 2.39×10^5, comparable to the largest Q-factor obtained by topological engineering, while the resonant wavelength is tuned by varying the lattice constant of the top perturbation layer. Our results hold great promise for exciting applications, such as sensors and filters.

Introduction

High-Q photonic nano-resonators constitute a core element to realize high-performance optoelectronic and photonic devices in modern optical communications. While very large Q-factors have been obtained with micro-ring resonators and micro-disks via the optical fiber excitation through in-plane near-field coupling[1], it is very challenging to achieve an ultrahigh Q-factor in experiments via free-space excitation. Resonant waveguide gratings and photonic crystal slab are viewed as an ideal platform to achieve high-Q guided-mode resonances (GMRs)[2–4], which can be accessed in free space. They have been widely used in in filtering[5–10], sensing[11,12], and wavefront shaping[13,14]. Although the Q-factors of GMRs in theory can be very high, the largest Q-factor in experiments has been so far limited by fabrication imperfections (i.e., roughness, disorder, non-uniformity) causing increased radiation loss. To date, most of reported Q-factors of GMR in experiments are ranged from few hundreds to thousands.

Recently, bound states in the continuum (BICs) has introduced a viable alternative to realize ultrahigh-Q resonances in a free space setting[15–18]. The giant field enhancement typically associated with large-Q factors can benefit applications ranging from lasing [19–21], sensing[22,23], strong coupling[24,25] to enhanced nonlinear harmonic generations[26–29]. Most of the quasi-BICs(QBICs)-based high-Q modes reported so far are achieved by patterning the high-index semiconductor thin film as a single nanoparticle[30–32] or an array of nanoparticles on substrate[15,16,33–36]. Typically, the Q-factors of QBICs are limited by scattering

loss caused by unavoidable fabrication imperfections (i.e., roughness, disorder). Also, substrate introduces the additional leaky channel and thus reduce the Q-factors of QBICs. Of course, ultrahigh-Q modes can still be constructed by carefully arranging the structure parameters. For example, topological BICs, arising from merging multiple BICs into a single one, are found to be less sensitive to fabrication imperfections[37–42]. However, achieving such a high Q-factor requires delicate engineering of the structure parameters, and may not always be compatible with other design goals. Moreover, the substrate has to be removed to satisfy the environment symmetry. In addition, generalizing this achievement to visible wavelengths is an outstanding challenge that may prove difficult due to materials and fabrication constraints. In real applications, it is desirable to develop a design strategy for realizing ultrahigh Q-resonance that can minimize the fabrication imperfection, mitigate the substrate effect, and does not need careful topological engineering.

In this work, we introduce a strategy to implement ultrahigh-Q guided-mode resonances in an all-dielectric metasurface without the need for topological engineering of the structure or introducing any symmetry breaking other than the discretization of translational symmetry. Instead of patterning the high-index layer to form a Mie resonator in a unit cell, we introduced an ultrathin perturbation layer (i.e., photoresist layer) on top of a multilayer-waveguide system so that guided modes are transformed into leaky modes that produce GMRs. The high Q-factors of GMRs can be easily realized as they show a linear dependence on the inverse perturbation square α^{-2}. The perturbation can be reduced to a very small value because the fabrication of such a device only involves spin-coating of resist and developing, enabling minimal perturbation by removing the roughness and disorder of the sample. The validity of such a design methodology is confirmed by patterning a low-index photoresist thin film on a standard SOI sample that serves as a simple waveguide system. The experimental results show that the Q-factor was as high as $2.39 \cdot 10^5$, comparable to the maximum Q-factor of topological BICs. In addition, the resonant wavelength was easily tuned by changing the period of the meta-waveguide system. This design strategy is robust and powerful in obtaining ultrahigh-Q resonances at arbitrary operating wavelengths because it can be generalized to any other waveguide system made of any different high refractive index ($n = 2 \sim 5$) as the core layer. Our results may find great potential in applications requiring ultrasharp spectral features, such as sensing and filtering.

Results And Discussion

We start by investigating the leaky modes of a multilayer waveguide structure, consisting of a high refractive index n_2 layer with finite thickness sandwiched between two semi-infinite layers with low refractive index being n_1 and n_3, respectively. Without loss of generality, we assume that the electric field component is perpendicular to the plane of structure, which is E//y. Such an open system supports a series of Fabry-Perot resonant modes with low-Q factors (See Section 1 in SM and Fig.S1). If we apply a virtual periodic boundary condition with arbitrary periods, in addition to the low-Q leaky modes such a simple geometry can also support guided modes (GMs) with an infinite Q-factor. Note that there are two ways of defining a periodic structure: a 1D grating or a 2D metasurface, as shown in Fig. 1a and Fig.S2.

The analytical solutions of the band-diagram for TE (E//y) and TM (H//y) modes are given in section 2 of supplementary materials and Fig.S3. Here, we mainly focus on the GMs at Γ point in the first Brillouin zone in momentum space. Alternatively, the eigenfrequency of these GMs can be calculated quickly with the commercial software COMSOL Multiphysics. For the 1D grating system, these GMs are designated as TE_{ml} (TM_{ml})[43,44], where m and l are the number of antinodes of the electric (magnetic) field in the x and z directions, respectively. Figure 1b-c shows two typical examples of GMs: modes TE_{21} and TE_{31}. These GMs can be transformed into GMRs by introducing an ultrathin low index metasurface on top of the high index layer. For example, when the top perturbation layer is patterned as a grating, GMs TE_{21} and TE_{31} are converted into symmetry-protected BIC mode TE_{21} and GMR TE_{31} with a finite Q-factor. If the symmetry of the top periodic structure is broken, BIC mode TE_{21} is reduced to QBIC. Note that GMs like TE_{21} and TE_{31} at the Γ point share a similar feature with symmetry protected BICs. When the periodic perturbation is introduced in the multilayer waveguide system, such GMs with infinite Q-factor are successfully converted into the GMRs with either infinite or finite Q-factor depending on the mode parity. If the perturbation approaches zero, the radiative decay rates of GMRs are reduced to zero. Rigorous derivation shows that their Q-factors are inversely proportional to the β^{-2} (see section 3 of SM), where β is perturbation parameter of the system. This is similar to the symmetry-protected BICs with $Q \infty \alpha^{-2}$(where α is the asymmetry parameter of unit cell). The GMs for the TM case are shown in Fig.S4. The following sections demonstrate that GMs provide much freedom and flexibility to design ultrahigh Q-factor resonance with a subwavelength meta-waveguide system at an arbitrary operating wavelength.

For simplicity, we use a three-layer structure air/Si/SiO_2 to design a high-Q resonance at 1550nm. Without loss of generality, the thickness of the middle layer Si is chosen as 220nm. The refractive index of Si and SiO_2 are set as 3.47 and 1.46, respectively. The virtual period is tuned to 548nm so that such a structure supports a GM at 1550nm. The resonant wavelength can be tuned to any other value by varying the period, which is discussed in the later section. By introducing a top perturbation layer that is patterned as either a grating or a metasurface, the GM evolves into a BIC or GMR depending on the structure's geometry and the mode's parity. Their band structures are plotted in Fig.S5-6. Here, it is worth noting that the refractive index of grating or metasurface can be any value as long as the top layer serves as a perturbation layer. As an example, the refractive index of the top layer is set as 1.46, matching the index of SiO_2. We first consider a simple grating structure shown in Fig. 2a and study the effect of width and thickness on the Q-factor of GMR. From Fig. 2b, it can be found that the Q-factor of the GMR TE_{31} is proportional to t^{-2} when the width of the grating is fixed as 200nm, similar to the observation in symmetry-protected BICs, where $Q \infty \alpha^{-2}$(where α is the asymmetry ratio). Such a relationship is well explained by perturbation theory[45] (see section 3 in supplementary materials). This is also confirmed by the reflection spectrum mapping as the thickness increases from 0 to 300nm (See Fig.S7).

Similarly, the Q-factor shows a linear dependence on w^{-2} or $(d-w)^{-2}$ for a given thickness, as confirmed in Fig. 2c. Thus, it can be safely concluded that the effective perturbation area or volume plays the dominant role in governing the Q-factors of GMRs. Moreover, the resonant wavelength remains almost

the same with the changing thickness or width because of low index nature of the top perturbation layer (See Fig.S7-8). As described in Fig. 1, except for the GMR TE_{31}, such a grating also supports a symmetry-protected BIC mode TE_{21} due to structural symmetry. Further breaking the symmetry can induce the transition from BIC to QBIC. For instance, by introducing an asymmetric air slit inside the rectangular nanowire, mode TE_{21} is successfully converted into the QBIC. Figure 2b shows the Q-factor of QBIC TE_{21} as a function of thickness. The case of TE_{31} is also plotted as a reference to make a comparison. Similar to the case of TE_{31} shown in Fig. 2b, the Q-factor of mode TE_{21} is proportional to t^{-2} when an asymmetric slit is introduced with g = 120nm and xc = 10nm. The left and right nanowires' widths are 110nm and 90nm, respectively. Besides, we find that the Q-factor of mode TE_{21} is more than one order of magnitude higher than that of mode TE_{31}. This is understandable because the perturbation required for symmetry-broken is much smaller for TE_{21} compared to mode TE_{31}. Such a general conclusion also can be generalized to the 3D metasurface. When the cuboid unit cell of the top perturbation layer is arranged as a square lattice, such a metasurface supports degenerate symmetry protected BICs (TE_{211} and TE_{121}) and GMRs (TE_{311} and TE_{131}). The degeneracy could be easily lifted by choosing the different lattice constants along x and y-axis (See Fig.S9). Further introducing in-plane broken symmetry leads to the transition from BICs into QBICs for TE_{211} mode. Figure 2g-i shows the Q-factor of GMRs TE_{311} and TE_{211} versus the thickness of top layer. Additionally, it is not surprising that Q-factor follows a similar trend as 1D grating, $Q \propto t^{-2}$. Moreover, such a 2D metasurface supports BICs or GMRs for TM cases (See Fig.S10). Here, it is necessary to point out that the top layer can also be patterned as a rectangular lattice with any other shape such as photonic crystal slab because it just functions as a weak perturbation layer.

Note that many GMs can be easily constructed with such a simple meta-waveguide system. We again consider the 1D grating structure shown in Fig. 1a with material parameters and geometry parameters given in Fig. 2a. Except for TE_{21} and TE_{31} mode, such a three-layer structure supports other high-order GMs. Figure 3a shows the field distribution of six GMs: TE_{21} and TE_{31}, TE_{22} and TE_{32}, TE_{41} and TE_{51}. Their resonant wavelengths are presented in Fig. 3b. Note that all of these modes are dominated by the zero-order diffraction. Of course, even higher-order GMs like TE_{42} and TE_{52} can be found. However, their Q-factor may decrease significantly due to the enhanced radiation from unwanted diffraction after the perturbation is introduced. Also, GMs may be designed at any pre-defined wavelength with different structure parameters and material parameters. For example, if the thickness of the Si layer is set as 220nm or 340nm, we can always tune the virtual period so that the resonant wavelengths of GM TE_{21} or TE_{31} could cover a broadband wavelength range from 1000nm to 1800nm, as displayed in Fig. 3c.

Similarly, from Fig. 3d, we found that the resonant wavelength can be tuned by varying the thickness of Si layer while the period is fixed as 450nm (or 550nm). One can also engineer the GM's wavelength by choosing materials with different refractive indices. For example, to design a GM at 1550nm, the period should be varied from 1000nm to 460nm when the refractive index n_2 increases from 2 to 4. The corresponding result is shown in Fig. 3e. To verify the robustness of such a design strategy in realizing ultrahigh-Q resonances, we calculate the Q-factor of GMR TE_{31} in a grating system for the middle layer

with various refractive index n_2. Indeed, all of the Q-factors decrease significantly with the increasing thickness of the top grating layer, as illustrated in Fig. 3f. Nevertheless, it is interesting that the Q-factor for high-index $n_2 = 3.5$ is almost one order higher than the low index $n_2 = 2.0$. This can be intuitively understood by the reduced index contrast between the substrate (or superstrate) and the sandwiched high-index layer, which leads to more energy radiation into substrate (or superstrate) instead of confining inside the high-index layer.

After gaining a solid understanding of designing ultrahigh-Q resonances from GMs, we move to the experimental demonstration of such a high-Q resonance. We fabricate a series of photonic crystal slab made of 330nm thick photoresist on an SOI substrate (220nm-Si/2μm-SiO_2/Si) using electron-beam lithography followed by developing process. Here, photo-resist layer instead of SiO_2 layer is patterned as perturbation layer. On the one hand, the photoresist has a low refractive index around 1.4. On the other hand, no other postprocessing (i.e., dry etching) is applied to the other layers so that higher sample quality is guaranteed.

Figure 4a shows the schematic drawing of the whole device, and Fig. 4b shows the scanning electron microscopy image of one typical fabricated sample. The lattice constants along x and y-axis are identical in this device. We first investigate the effect of hole size on the Q-factor by fixing the lattice constant as 545nm but varying the hole radius. Eigenmode calculations indicate that such a structure can support degenerate GMRs TE_{311} and TE_{131} at around 1550nm. It also supports symmetry protected BICs TE_{211} and TE_{121}. However, they cannot be excited at normal incidence unless the in-plane symmetry is broken. We measured the scattering spectrum from these samples by using a custom-made cross-polarization measurement system (See Fig. S11). The relevant results are put in Fig. 4d-f. It can be observed from Fig. 4d that shrinking the size of the hole on the top perturbation layer leads to the narrowing of resonance linewidth and slight redshift of resonance. We retrieved the quality factor and resonant wavelength of these high-Q resonances by fitting them to a Fano-profile. Figure 4e shows one example of Fano fitting for R = 72nm. The measured Q-factor for structure with different hole sizes is presented in Fig. 4f, where the highest Q-factor is up to $2.39 \cdot 10^5$ at R = 72nm. Such a high Q-factor is comparable to the record-high Q-factors in a topological metasurface[40]. Nevertheless, our approach involves only patterning the top resist layer without the need for carefully engineering the topological features. Also, the calculated Q-factor is plotted as a reference and is found to show an excellent agreement with the experiment measurement. In fact, we also fabricate the sample with an even smaller radius R = 35nm. However, it becomes very challenging to get an even higher Q-factor in experiment because the peak cannot be distinguished from the noise or background. Further optimization of the measurement system is needed. Such an ultrahigh-Q factor can be attributed to two factors: small hole radius and shallow hole with partial unetched resist film underneath. After taking both factors into account, the calculated Q is an order of million for such a size.

Finally, to demonstrate the tunability of resonant wavelength, we fabricate five samples with the period varying from 535nm to 555nm while their hole radii are fixed as 80nm. The scattering spectra are plotted

in Fig. 5g. Indeed, the resonant peaks show a linear dependence on the period, matching very well to the theoretical calculation. In addition, all of the measured Q-factor are ranged between $1.0{\cdot}10^5$ and $2{\cdot}10^5$. Note that TE_{311} and TE_{131} are degenerate for the identical lattice constants along the x and y-axis. This degeneracy can be lifted by employing a rectangular lattice with different p_x and p_y. Thus, high-Q resonance could be implemented at a different wavelength by switching the polarization (See Fig.S12). In other words, even a single structure can support two high-Q modes at different wavelengths for x and y-polarization. In addition to reducing the hole size, this ultrahigh-Q mode may be enabled by using an ultrathin material as perturbation layer. The recently developed two-dimensional (2D) materials, especially 2D transition metal dichalcogenides (TMDCs)[46,47], are ideal candidates for realizing atomically thin film below 10nm. Moreover, such a 2D TMDC multilayer with thickness below 10nm can be easily patterned by ICP etching. Although the refractive index of TMDC is a bit high (n = 3∼4.5 in the NIR), their atomically thin nature makes them an excellent candidate as a perturbation layer. We expect a high-quality thin film like TMDCs multilayer and mature fabrication process could help to realize an ultrahigh-Q factor larger than 10^6 or even more.

Conclusion

In summary, we theoretically proposed and experimentally demonstrated high-Q guided resonances in a meta-waveguide system. The designing strategy builds upon adding a perturbation layer (i.e., photoresist) on top of a conventional waveguide system, which converts GMs into the BICs or GMRs. The Q-factors of GMRs strongly depend on the perturbation of meta-waveguide system, suggesting an easy and viable way of realizing ultrahigh-Q resonances without resorting to carefully topological engineering. Ultrahigh Q-factor of GMR can be made because fabricating this structure only involves resist-coating and developing but no deep etching process, successfully eliminating the potential roughness and disorder of the sample and enabling the tiny perturbation in real devices. We experimentally demonstrate the feasibility of this design strategy in achieving the high-Q resonances at around 1.55μm by fabricating a thin photoresist layer photonic crystal slab on top of 220nm Si/2um SiO_2/Si (standard SOI sample). The maximum Q-factor is up to $2.39{\cdot}10^5$. Also, the resonant wavelength can be tuned by varying the lattice constants of top layer. Furthermore, by choosing different lattice constants along the x and y-axis, we realized polarization-dependent GMRs. Our findings may open a new avenue of designing optoelectronic and photonic devices where ultrasharp spectral features may improve their performances, such as biosensors and filters.

Materials And Method

Numerical simulation

The eigenmodes of meta-waveguide are calculated by commercial software Comsol Multiphysics based on finite-element-method (FEM). The reflection and transmission spectra of meta-structures are calculated by rigorous-coupled wave analysis (RCWA).

Fabrication

Our devices were fabricated on a silicon-on-insulator (SOI) wafer with a 220-nm silicon layer and 2-um-thick buried layer. The SOI was firstly coated with the 330-nm-thick resist layer (ZEP520). Then, the device patterns were defined on the resist by electron-beam lithography. After that, the devices were carefully developed and fixed by dimethyl benzene and iso-Propyl alcohol liquors, respectively.

Optical Characterization

The incident light source was a tunable telecommunication laser(santec TSL-550), the wavelength of which could be tuned from 1480nm to 1630nm. Light first passed though the polarizer, lens and beam splitter, and then focused on the rear focal plane of the objective lens(10X), to make sure the incident light on the sample was close to normal incidence. The reflected signal was collected by a photodiode(PDA10DT-EC), which could be switched to a CCD to locate the sample. A lock-in amplifier with the help of chopper(SR540) was connected to the photodiode to pick out the signal from the background noise. A pair of orthogonal polarizers were placed at the front and the middle part of the light path, to introduce cross-polarization which could efficiently decrease the impact from background reflection and promote relative intensity of the signal.

Declarations

Acknowledgements

L. Huang and A. E. Miroshnichenko were supported by the Australian Research Council Discovery Project (DP200101353) and the UNSW Scientia Fellowship program. C. Zhou was supported by the National Natural Science Foundation of China (Grants No. 12004084 and 12164008). R. Jin, G. Li and X. Chen were supported by National Key Research and Development Program of China (2018YFA0306200 and 2017YFA0205800), National Natural Science Foundation of China (61875218, 61991440, and 91850208), Youth Innovation Promotion Association of Chinese Academy of Sciences (2017285), Strategic Priority Research Program of Chinese Academy of Sciences (XDB43010200); Shanghai Rising-Star Program (20QA1410400), Natural Science Foundation of Zhejiang Province (LR22F050004), Shanghai Science and Technology Committee (20JC1416000), and Shanghai Municipal Science and Technology Major Project (2019SHZDZX01).

Author Contributions

L. H and A. E. M conceived the idea. L. H performed the theoretical calculation and numerical simulation. C. Z fabricated the sample and help with numerical simulations. R. J and G. L carried out the morphology characterization, built up the optical system and implemented the measurement. A. O, L. X and F. D helped with the numerical simulation. X. C, W. L, A. A, and A. E. M supervised the project. L. H and A. E. M prepared the manuscript with the input from all authors.

References

1. Armani, D. K., Kippenberg, T. J., Spillane, S. M. & Vahala, K. J. Ultra-high-Q toroid microcavity on a chip. *Nature* **421**, 925–928 (2003).

2. Quaranta, G., Basset, G., Martin, O. J. F. & Gallinet, B. Recent Advances in Resonant Waveguide Gratings. *Laser Photon. Rev.* **12**, 1800017 (2018).

3. Fan, S. & Joannopoulos, J. D. Analysis of guided resonances in photonic crystal slabs. *Phys. Rev. B* **65**, 235112 (2002).

4. Lee, J., Zhen, B., Chua, S.-L., Shapira, O. & Soljačić, M. Fabricating centimeter-scale high quality factor two-dimensional periodic photonic crystal slabs. *Opt. Express* **22**, 3724–3731 (2014).

5. Liu, Z. S., Tibuleac, S., Shin, D., Young, P. P. & Magnusson, R. High-efficiency guided-mode resonance filter. *Opt. Lett.* **23**, 1556–1558 (1998).

6. Niraula, M., Yoon, J. W. & Magnusson, R. Single-layer optical bandpass filter technology. *Opt. Lett.* **40**, 5062–5065 (2015).

7. Peng, S. & Morris, G. M. Resonant scattering from two-dimensional gratings. *J. Opt. Soc. Am. A* **13**, 993–1005 (1996).

8. Peng, S. & Morris, G. M. Experimental demonstration of resonant anomalies in diffraction from two-dimensional gratings. *Opt. Lett.* **21**, 549–551 (1996).

9. Wang, S. S. & Magnusson, R. Theory and applications of guided-mode resonance filters. *Appl. Opt.* **32**, 2606–2613 (1993).

10. Tibuleac, S. & Magnusson, R. Reflection and transmission guided-mode resonance filters. *J. Opt. Soc. Am. A* **14**, 1617–1626 (1997).

11. Romano, S. *et al.* Optical Biosensors Based on Photonic Crystals Supporting Bound States in the Continuum. *Materials (Basel).* **11**, (2018).

12. Zhou, Y. *et al.* High-Q guided mode resonance sensors based on shallow sub-wavelength grating structures. *Nanotechnology* **31**, 325501 (2020).

13. Lawrence, M. *et al.* High quality factor phase gradient metasurfaces. *Nat. Nanotechnol.* **15**, 956–961 (2020).

14. Klopfer, E., Lawrence, M., Barton, D. R., Dixon, J. & Dionne, J. A. Dynamic Focusing with High-Quality-Factor Metalenses. *Nano Lett.* **20**, 5127–5132 (2020).

15. Hsu, C. W. *et al.* Observation of trapped light within the radiation continuum. *Nature* **499**, 188–191 (2013).

16. Bulgakov, E. N. & Sadreev, A. F. Bloch bound states in the radiation continuum in a periodic array of dielectric rods. *Phys. Rev. A* **90**, 53801 (2014).

17. Hsu, C. W., Zhen, B., Stone, A. D., Joannopoulos, J. D. & Soljačić, M. Bound states in the continuum. *Nat. Rev. Mater.* **1**, 16048 (2016).

18. Sadreev, A. F. Interference traps waves in an open system: bound states in the continuum. *Reports Prog. Phys.* **84**, 55901 (2021).

19. Kodigala, A. *et al.* Lasing action from photonic bound states in continuum. *Nature* **541**, 196 (2017).

20. Huang, C. *et al.* Ultrafast control of vortex microlasers. *Science (80-.).* **367**, 1018 LP-1021 (2020).

21. Yu, Y. *et al.* Ultra-coherent Fano laser based on a bound state in the continuum. *Nat. Photonics* **15**, 758–764 (2021).

22. Romano, S. *et al.* Ultrasensitive Surface Refractive Index Imaging Based on Quasi-Bound States in the Continuum. *ACS Nano* **14**, 15417–15427 (2020).

23. Andreas, T. *et al.* Imaging-based molecular barcoding with pixelated dielectric metasurfaces. *Science (80-.).* **360**, 1105–1109 (2018).

24. Kravtsov, V. *et al.* Nonlinear polaritons in a monolayer semiconductor coupled to optical bound states in the continuum. *Light Sci. Appl.* **9**, 56 (2020).

25. Al-Ani, I. A. M., As'Ham, K., Huang, L., Miroshnichenko, A. E. & Hattori, H. T. Enhanced Strong Coupling of TMDC Monolayers by Bound State in the Continuum. *Laser Photon. Rev.* **15**, 2100240 (2021).

26. Xu, L. *et al.* Dynamic Nonlinear Image Tuning through Magnetic Dipole Quasi-BIC Ultrathin Resonators. *Adv. Sci.* **6**, 1802119 (2019).

27. Koshelev, K. *et al.* Subwavelength dielectric resonators for nonlinear nanophotonics. *Science (80-.).* **367**, 288 LP-292 (2020).

28. Liu, Z. *et al.* High-Q Quasibound States in the Continuum for Nonlinear Metasurfaces. *Phys. Rev. Lett.* **123**, 253901 (2019).

29. Vabishchevich, P. P. *et al.* Enhanced Second-Harmonic Generation Using Broken Symmetry III–V Semiconductor Fano Metasurfaces. *ACS Photonics* **5**, 1685–1690 (2018).

30. Rybin, M. V *et al.* High-Q Supercavity Modes in Subwavelength Dielectric Resonators. *Phys. Rev. Lett.* **119**, 243901 (2017).

31. Huang, L., Xu, L., Rahmani, M., Neshev, D. & Miroshnichenko, A. E. Pushing the limit of high-Q mode of a single dielectric nanocavity. *Adv. Photonics* **3**, (2021).

32. Bogdanov, A. A. *et al.* Bound states in the continuum and Fano resonances in the strong mode coupling regime. 1–12 (2018). doi:10.1117/1.AP.1.1.016001

33. Koshelev, K., Lepeshov, S., Liu, M., Bogdanov, A. & Kivshar, Y. Asymmetric Metasurfaces with High-Q Resonances Governed by Bound States in the Continuum. *Phys. Rev. Lett.* **121**, 193903 (2018).

34. Tuz, V. R. *et al.* High-quality trapped modes in all-dielectric metamaterials. *Opt. Express* **26**, 2905–2916 (2018).

35. Cui, C. *et al.* Multiple Fano Resonances in Symmetry-Breaking Silicon Metasurface for Manipulating Light Emission. *ACS Photonics* **5**, 4074–4080 (2018).

36. Campione, S. *et al.* Broken Symmetry Dielectric Resonators for High Quality Factor Fano Metasurfaces. *ACS Photonics* **3**, 2362–2367 (2016).

37. Bulgakov, E. N. & Maksimov, D. N. Bound states in the continuum and polarization singularities in periodic arrays of dielectric rods. *Phys. Rev. A* **96**, 63833 (2017).

38. Yuan, L. & Lu, Y. Y. Strong resonances on periodic arrays of cylinders and optical bistability with weak incident waves. *Phys. Rev. A* **95**, 23834 (2017).

39. Bulgakov, E. N. & Maksimov, D. N. Topological Bound States in the Continuum in Arrays of Dielectric Spheres. *Phys. Rev. Lett.* **118**, 267401 (2017).

40. Jin, J. *et al.* Topologically enabled ultrahigh-Q guided resonances robust to out-of-plane scattering. *Nature* **574**, 501–504 (2019).

41. Zhen, B., Hsu, C. W., Lu, L., Stone, A. D. & Soljačić, M. Topological Nature of Optical Bound States in the Continuum. *Phys. Rev. Lett.* **113**, 257401 (2014).

42. Doeleman, H. M., Monticone, F., den Hollander, W., Alù, A. & Koenderink, A. F. Experimental observation of a polarization vortex at an optical bound state in the continuum. *Nat. Photonics* **12**, 397–401 (2018).

43. Huang, L., Yu, Y. & Cao, L. General Modal Properties of Optical Resonances in Subwavelength Nonspherical Dielectric Structures. *Nano Lett.* **13**, 3559–3565 (2013).

44. Huang, L. *et al.* Atomically Thin MoS2 Narrowband and Broadband Light Superabsorbers. *ACS Nano* **10**, 7493–7499 (2016).

45. Yuan, L. & Lu, Y. Y. Perturbation theories for symmetry-protected bound states in the continuum on two-dimensional periodic structures. *Phys. Rev. A* **101**, 43827 (2020).

46. Yu, Y. *et al.* Controlled Scalable Synthesis of Uniform, High-Quality Monolayer and Few-layer MoS2 Films. *Sci. Rep.* **3**, 1866 (2013).

47. Huang, L. *et al.* Enhanced light–matter interaction in two-dimensional transition metal dichalcogenides. *Reports Prog. Phys.* **85**, 46401 (2022).

Figures

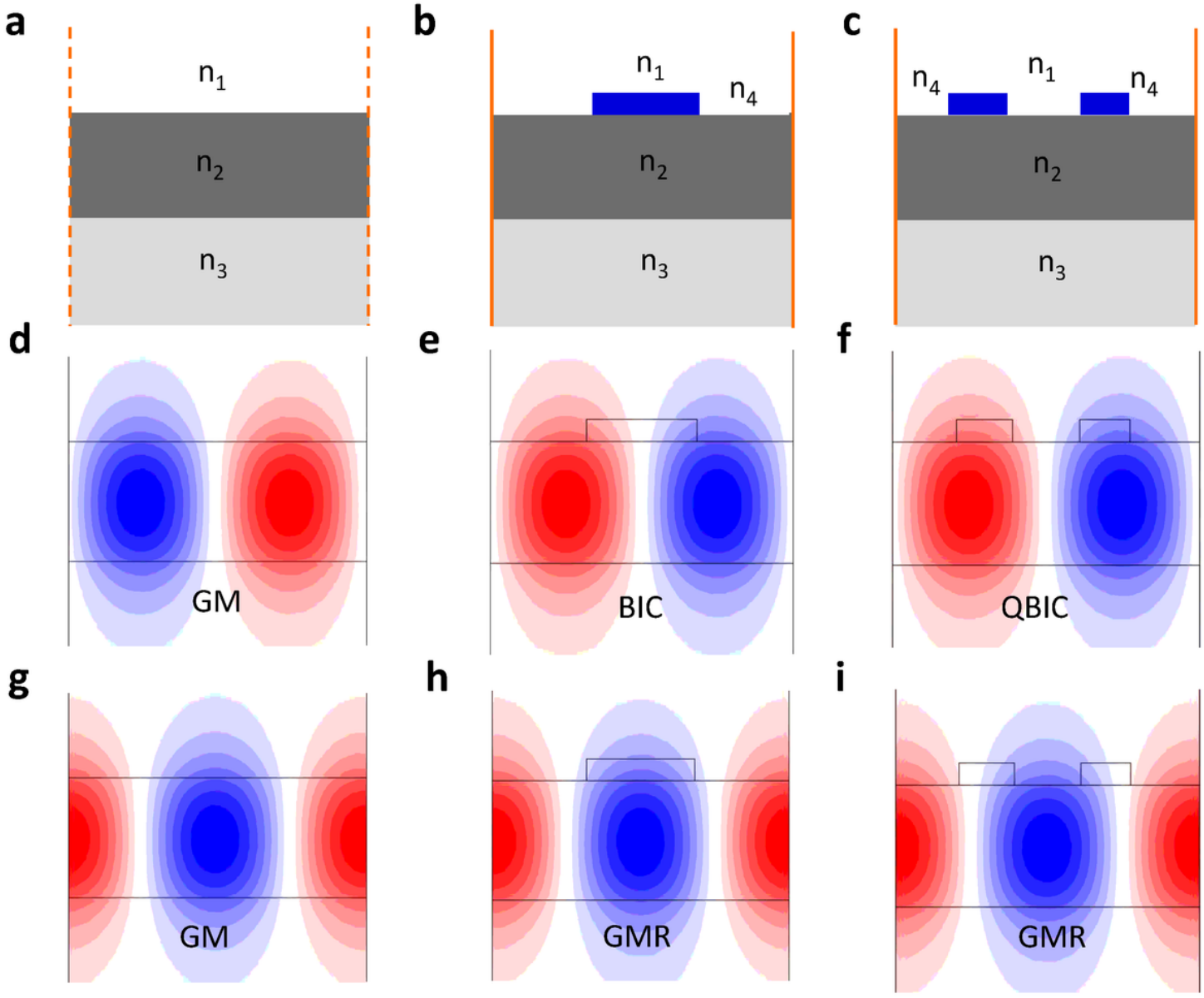

Figure 1

Designing strategy of high-Q GMRs. a-c, schematic drawing of three-layer waveguide system (a), and meta-waveguide system with top perturbation layer as simple grating (b) and compound grating (c) on the top. d and g are two examples of GMs. e and h are symmetry protected BICs and GMRs in the simple grating. f and i are GMRs for compound grating.

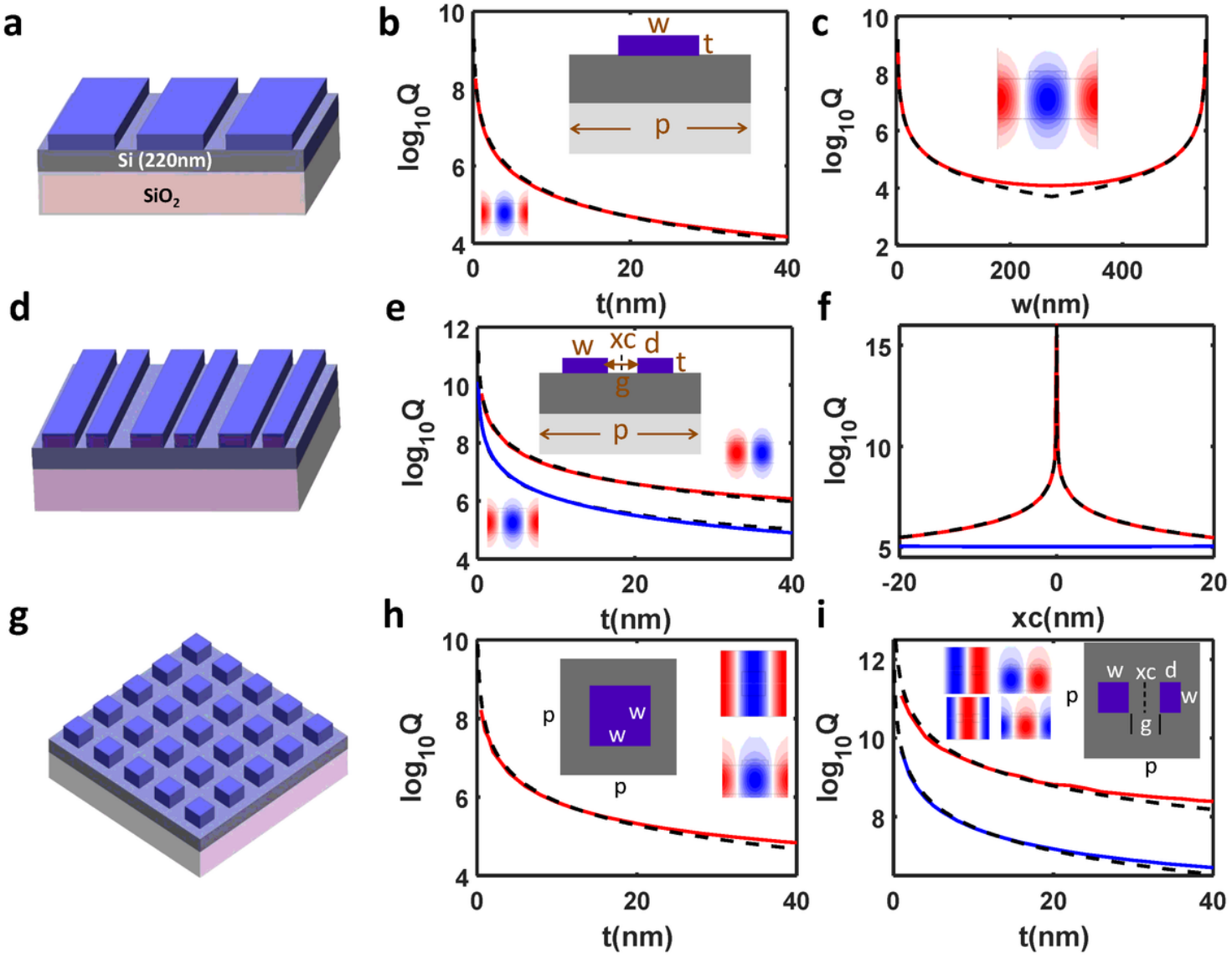

Figure 2

High-Q GMRs. a, schematic drawing of a meta-waveguide system made of an ultrathin SiO_2 grating on top of 220nm-Si on SiO_2 substrate. b, The Q-factor of GMR mode TE_{31} vs thickness of top perturbation layer. Solid and dashed lines are numerically calculated Q-factor and fitting Q-factor. The structure parameters are p=548nm and w=200nm. c, The Q-factor of GMR mode TE_{31} vs grating's width. The structure parameters are p=548nm and t=40nm. d, schematic drawing of a meta-waveguide system made of an ultrathin SiO_2 compound grating on top of 220nm-Si on SiO_2 substrate. e, The Q-factor of GMRs TE_{21} and TE_{31} vs thickness of top perturbation layer. The structure parameters are p=548nm, w=110nm, d=90nm, g=120nm, xc=10nm. f, The Q-factor of GMRs TE_{21} and TE_{31} vs gap center xc. The

structure parameters are p=548nm, w+d=200nm, g=120nm. g, schematic drawing of a meta-waveguide system made of an ultrathin SiO_2 metasurface on top of 220nm-Si on SiO_2 substrate. h, The Q-factor of GMR mode TE_{311} vs the thickness of top perturbation layer. The structure parameters are p=548nm, w=200nm. i, The Q-factor of GMR modes TE_{211} and TE_{311} vs top layer thickness. The structure parameters are p=548nm, w+d=200nm, g=120nm.

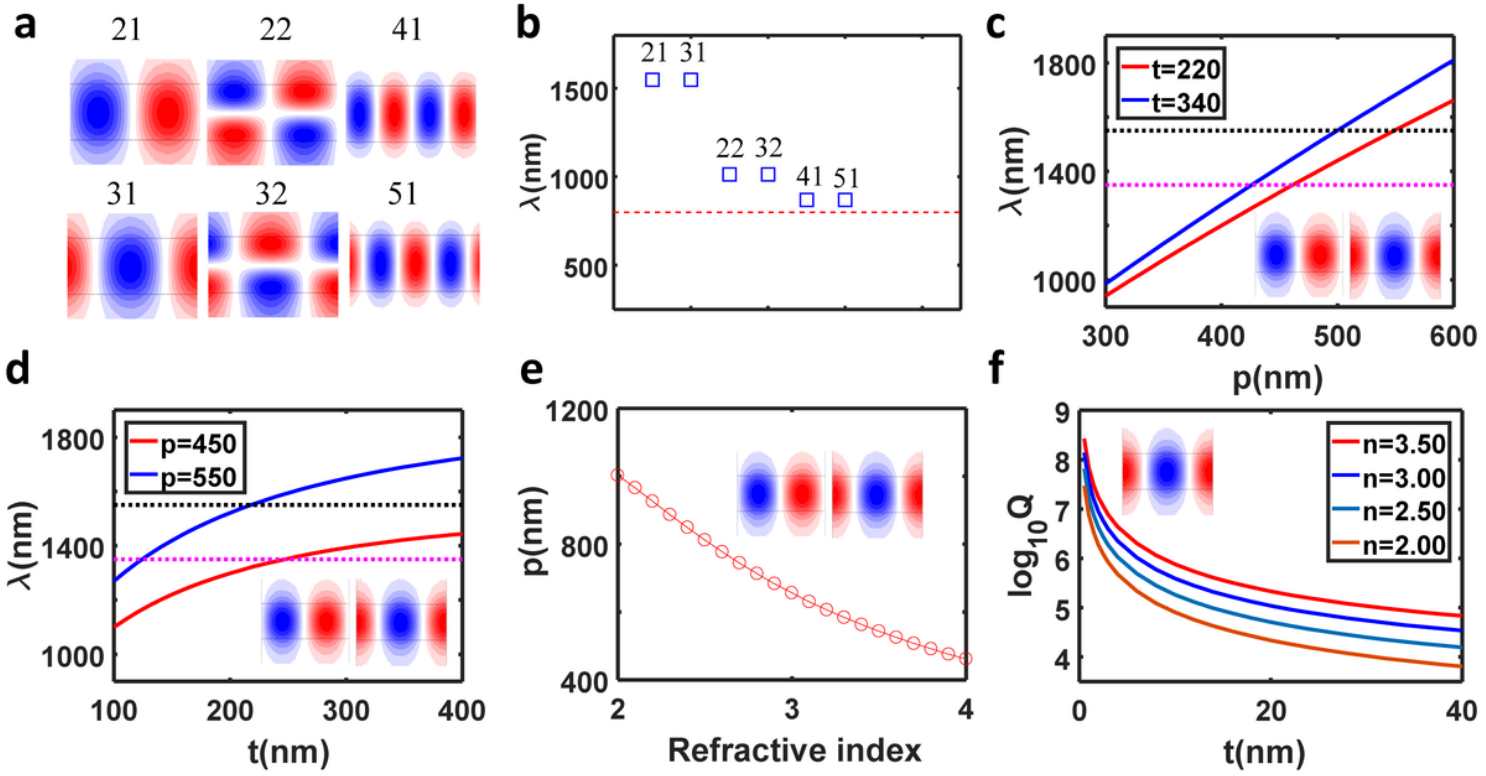

Figure 3

Designing GMs at arbitrary wavelength. a, eigenfield distribution Ey of six GMs in the 220nm-Si on SiO_2 substrate with virtual period p=548nm. b, resonant wavelengths of six GMs. c, resonant wavelength engineering through the virtual period. d, resonant wavelength engineering through the thickness of Si layer. e, virtual period of three-layer waveguide as a function of refractive index of middle layer. Here, the resonant wavelengths of two GMs are fixed as 1550nm. f, Q-factors of GMR TE_{31} vs the thickness of top perturbation layer for the meta-waveguide system with varied refractive index of middle layer.

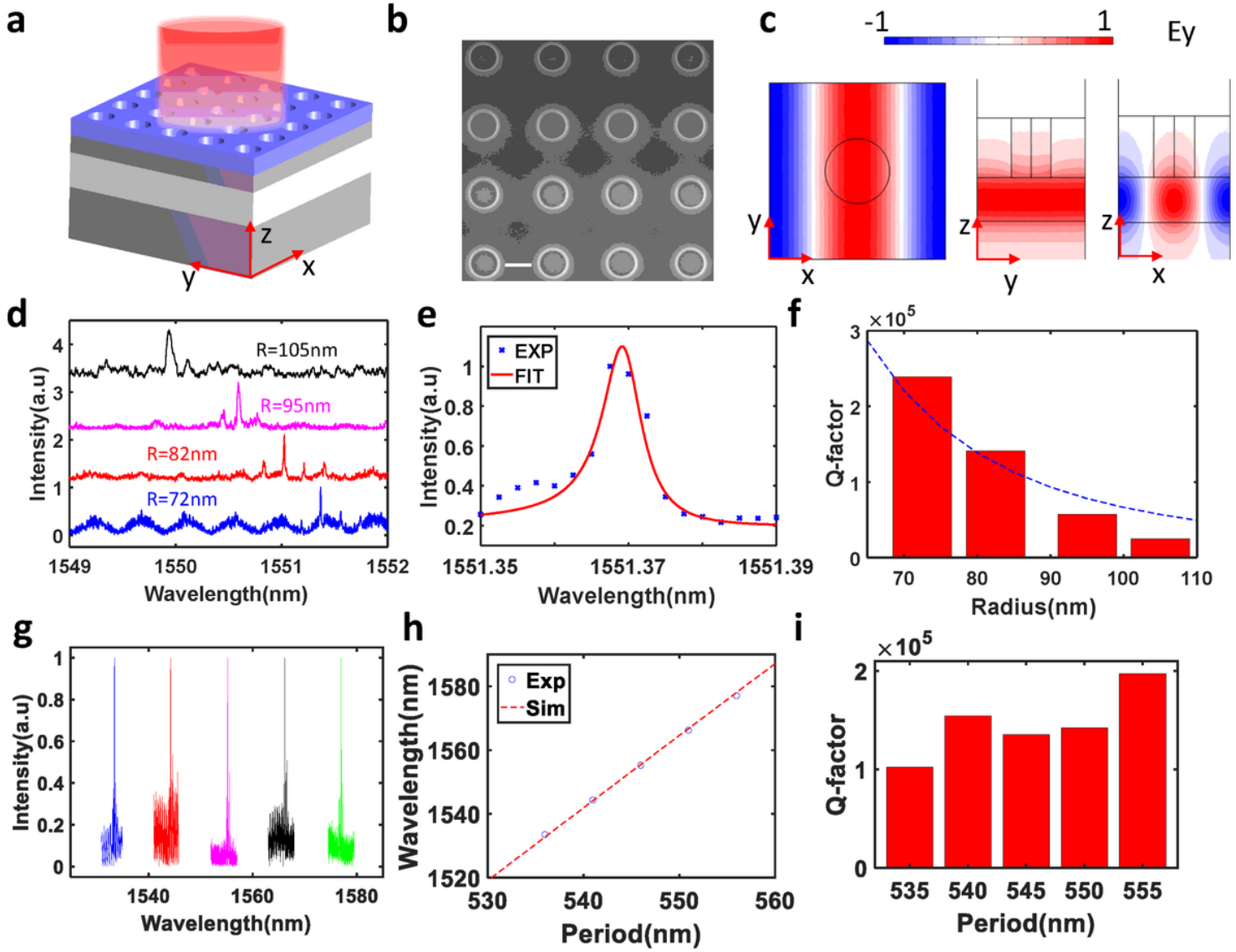

Figure 4

Experimental demonstration of high-Q resonance based on GMs. a, schematic drawing of a 3D meta-waveguide system. The top perturbation is patterned as photonic crystal slab with air hole. b, SEM image of a fabricated meta-waveguide system. the scale bar in white is 200nm c, eigenfield distribution for GMRs TE_{311}. d, measured reflection spectra for four fabricated samples with fixed period 545nm but varied hole radius from 72nm to 105nm. e, Fano-fitting for reflection spectrum for hole radius R=72nm. f, retrieved Q-factors vs radius for mode TE_{311}, dash line is the simulated Q-factor. g, measured reflection spectra for meta-waveguide system when periods change from 535nm to 555nm. h, Comparison between calculated and measured resonant wavelength. i, retrieved Q-factor vs period.

Supplementary Files

This is a list of supplementary files associated with this preprint. Click to download.

- SupportingMaterials.docx